

## Synthesis, structure and spectral properties of 9-diaryl-amino-substituted acridines



Viacheslav A. Sazhnikov<sup>a,\*</sup>, Artem A. Khlebunov<sup>a</sup>, Sergey K. Sazonov<sup>a</sup>, Artem I. Vedernikov<sup>a</sup>, Andrei A. Safonov<sup>a</sup>, Alexander A. Bagatur'yants<sup>a</sup>, Lyudmila G. Kuz'mina<sup>b</sup>, Judith A.K. Howard<sup>c</sup>, Sergey P. Gromov<sup>a,\*</sup>, Michael V. Alfimov<sup>a</sup>

<sup>a</sup>Photochemistry Center, Russian Academy of Sciences, 7A-1 Novatorov Str., Moscow 119421, Russian Federation

<sup>b</sup>N.S. Kurnakov Institute of General and Inorganic Chemistry, Russian Academy of Sciences, 31 Leninskiy Prosp., Moscow 119991, Russian Federation

<sup>c</sup>Chemistry Department, Durham University, South Road, Durham DH1 3LE, UK

### HIGHLIGHTS

- Three 9-(diphenylamino)acridine dyes of the donor–acceptor type were synthesized.
- The acceptor and donor fragments are close to perpendicularity in the neutral forms of the dyes.
- The fluorescence bands of the dyes are red-shifted as compared to other known 9-aminoaryl-substituted acridines.
- The synthesized dyes exhibit a significant solvatochromic effect and can be used as fluorescent chemosensors.
- Structural features and electronic properties of the dyes are accurately described within the TD-DFT framework.

### ARTICLE INFO

#### Article history:

Received 27 July 2012

Received in revised form 5 August 2013

Accepted 1 September 2013

Available online 11 September 2013

#### Keywords:

Acridine derivatives

X-ray structures

Fluorescence

Solvatochromism

DFT calculations

### ABSTRACT

The synthesis of three 9-diaryl-amino-substituted acridines is reported. The compounds of the donor–acceptor type – *N,N*-diphenylacridin-9-amine (**1**), 2,7-dimethyl-*N,N*-bis(4-methylphenyl)acridin-9-amine (**2**), and 2,7-bis(1-methyl-1-phenylethyl)-*N,N*-bis[4-(1-methyl-1-phenylethyl)phenyl]acridin-9-amine (**3**) were characterized by IR, <sup>1</sup>H and <sup>13</sup>C NMR, mass-spectral and elemental analysis. The crystal structures of compounds **1–3** and their protonated forms were determined by X-ray diffraction analysis. The absorption and fluorescence spectra were measured in various solvents. Solvatochromic shifts and dependence of the fluorescence quantum yields on the solvent polarity and protonation suggest the use of these compounds as chemical sensors. An example of a sensor material based on compound **2** is presented. Density functional theory calculations of the structures and time-dependent density functional theory calculations of the gas-phase excitation and emission energies of **1** were performed at the PBE0/SVP level of theory.

© 2013 Elsevier B.V. All rights reserved.

### 1. Introduction

Acridine derivatives are known to be one of the oldest classes of bioactive compounds [1]. In particular, proflavine and 9-aminoacridine were earlier widely used as antibacterial agents, whereas various derivatives of 9-arylaminoacridines are presently being studied as anticancer drugs [2,3]. The biological activity of the acridines is based on the ability of acridine moiety to intercalate between base pairs of double-stranded DNA through  $\pi$ – $\pi$  interactions that leads to alteration in the cellular machinery [4]. In the case of 9-arylami-

noacridines, the formation of ternary drug/DNA/enzyme complexes was stated [2,5]. In these complexes, the acridine moiety and aniline ring are suggested to be the DNA-binding and the enzyme-binding domains, respectively.

The photophysical properties of acridines have been widely investigated, both experimentally and theoretically [6–19,20–26]. In particular, 9-aryl- and 9-aminoaryl-substituted acridine and acridinium ion systems have received much attention because their photoexcitation was shown to result in the intramolecular electron transfer [9,11,12,14,15,18,4,22–24]. The most interesting photophysical and structural effects were demonstrated for 9-mesityl-10-methylacridinium ion [4,25,26] exhibiting an unusually long-lived electron transfer state on photoexcitation.

Because intramolecular charge transfer (ICT) states may differ markedly from the parent ground states in their molecular

\* Corresponding authors. Tel.: +7 495 9350119 (V.A. Sazhnikov), +7 495 9350116 (S.P. Gromov); fax: +7 495 9361255.

E-mail addresses: [sazhnikov@yandex.ru](mailto:sazhnikov@yandex.ru) (V.A. Sazhnikov), [spgromov@mail.ru](mailto:spgromov@mail.ru) (S.P. Gromov).

structure, structural changes accompanying ICT in 9-aminoarylacridines and corresponding acridinium ions were widely discussed in the framework of the twisted intramolecular charge transfer (TICT) model [15,18,22,23].

In our earlier study [27], we have briefly described the photoinduced synthesis of 9-diphenylamino-substituted acridine **1**. More recently [28], it was shown that its methyl derivative **2** exhibits a well-pronounced solvatochromic effect comparable with that of well-known dye Nile Red. This feature of **2** was used to develop polymer layers sensitive to vapors of polar solvents such as acetone or ethanol [29]. Protonated **2** was used as molecular sensor for recognition of ammonia vapor [30].

In order to better understand the relationship between the structure of 9-diarylamino-substituted acridines and their absorption and fluorescent properties, we have performed X-ray diffraction analysis and carried out detailed spectroscopic studies of three acridine derivatives **1–3** in their neutral and protonated forms. In addition, DFT calculations of the structures and TD-DFT calculations of the gas-phase excitation and emission energies of neutral and protonated **1** were performed at the PBE0/SVP level of theory.

## 2. Experimental

### 2.1. General

All the solvents for optical studies (spectroscopic grade) were purchased from Aldrich. Carbon tetrabromide, diphenylamine, di-*p*-tolylamine, di[4-(1-methyl-1-phenylethyl)phenyl]amine, fluorescein (for fluorescence studies) were used as received (Fluka, Aldrich, Merck).

The melting points (uncorrected) were measured in capillaries on a Mel-Temp II instrument. The  $^1\text{H}$  and  $^{13}\text{C}$  NMR spectra were recorded on a Bruker DRX500 spectrometer (500.13 and 125.76 MHz, respectively) in  $\text{CDCl}_3$  and  $\text{C}_6\text{D}_6$  at 25 °C using the signal from the solvents as the internal standards ( $\delta_{\text{H}}$  7.27 and 7.15,  $\delta_{\text{C}}$  77.00 and 128.00, respectively). The chemical shifts were measured with an accuracy of 0.01 ppm and the spin–spin coupling constants were determined with an accuracy of 0.1 Hz. The mass spectra were obtained on a Varian MAT 311A instrument using a direct inlet system; the ionization energy was 70 eV. High-resolution ESI mass spectra were measured on a Bruker Daltonics MicroTOF II instrument in the range of  $m/z = 50\text{--}3000$  for positive ions (MeCN solution inlet, nitrogen gas flow, 4500 V capillary voltage). Elemental analyses were performed at the Laboratory of Microanalysis of the A.N. Nesmeyanov Institute of Organoelement Compounds of the Russian Academy of Sciences (Moscow).

### 2.2. Synthesis of acridine derivatives **1–3** (general procedure)

A solution of a mixture of diarylamine (6 mmol) and carbon tetrabromide (330 mg, 1 mmol) in hexane (50 mL) was placed in Pyrex bulb and irradiated with sunlight for 4 weeks (Scheme 1). The purple precipitate thus formed (hydrobromide of **1–3**) was decanted, dissolved in benzene, washed with  $\text{NaHCO}_3$  solution (aq, sat.) and evaporated *in vacuo*. The residue was purified by column chromatography on aluminium oxide (90 neutral, 0.063–0.200 mm, Merck) using a 5:1 benzene–EtOAc mixture. The compound **1–3** was re-crystallized from MeCN.

#### 2.2.1. *N,N*-Diphenylacridin-9-amine (**1**)

*N,N*-Diphenylacridin-9-amine (**1**) was additionally purified from an impurity of triphenylmethane dye on the stage of hydrobromide salt separation. The solid hydrobromide of **1** was extracted with acetone (3 × 20 mL), the mother solution was

evaporated *in vacuo* and the residue then was purified as described in Section 2.2. Compound **1** was obtained as a yellow crystalline powder (yield 19%); m.p. 235–236 °C.  $^1\text{H}$  NMR ( $\text{CDCl}_3$ )  $\delta$ : 6.97 (t, 2 H, 2 H(4'),  $J = 7.3$  Hz), 7.07 (d, 4 H, 2 H(2'), 2 H(6'),  $J = 8.6$  Hz), 7.21 (t, 4 H, 2 H(3'), 2 H(5'),  $J = 7.9$  Hz), 7.41 (m, 2 H, H(3), H(6)), 7.74 (m, 2 H, H(2), H(7)), 8.09 (d, 2 H, H(4), H(5),  $J = 8.6$  Hz), 8.30 (d, 2 H, H(1), H(8),  $J = 9.2$  Hz) ppm.  $^{13}\text{C}$  NMR ( $\text{CDCl}_3$ )  $\delta$ : 121.09 (4 C), 122.20 (2 C), 124.59 (2 C), 125.34 (2 C), 126.45 (2 C), 129.43 (4 C), 130.11 (4 C), 147.58 (2 C), 147.77 (C(9)), 150.80 (2 C) ppm. MS  $m/z$ : 346 [ $\text{M}^+$ ] (100), 267 (4), 242 (5), 177 (4), 167 (5), 148 (5), 101 (8), 84 (6), 69 (5), 57 (10). Calcd. for  $\text{C}_{25}\text{H}_{18}\text{N}_2 \cdot 0.6\text{H}_2\text{O}$ : C 84.05, H 5.42, N 7.84; found: C 83.95, H 5.26, N 7.70%.

#### 2.2.2. 2,7-Dimethyl-*N,N*-bis(4-methylphenyl)acridin-9-amine (**2**)

2,7-Dimethyl-*N,N*-bis(4-methylphenyl)acridin-9-amine (**2**) was obtained as a yellow crystalline powder (yield 16%); m.p. 178–179 °C.  $^1\text{H}$  NMR ( $\text{C}_6\text{D}_6$ )  $\delta$ : 2.00 (s, 6 H, 2 Me), 2.02 (s, 6 H, 2 Me), 6.78 (d, 4 H, 2 H(2'), 2 H(6'),  $J = 8.4$  Hz), 7.00 (d, 4 H, 2 H(3'), 2 H(5'),  $J = 8.4$  Hz), 7.17 (dd, 2 H, H(3), H(6),  $J = 8.6$  Hz,  $J = 1.8$  Hz), 8.03 (br.s, 2 H, H(1), H(8)), 8.45 (d, 2 H, H(4), H(5),  $J = 8.6$  Hz) ppm.  $^{13}\text{C}$  NMR ( $\text{C}_6\text{D}_6$ )  $\delta$ : 20.54 (2 Me), 22.01 (2 Me), 121.11 (4 C), 122.98 (2 C), 126.16 (2 C), 130.36 (4 C), 131.10 (2 C), 131.18 (2 C), 132.40 (2 C), 136.47 (2 C), 146.09 (2 C), 146.18 (C(9)), 150.28 (2 C) ppm. MS  $m/z$ : 402 [ $\text{M}^+$ ] (100), 296 (6), 295 (5), 282 (3), 191 (3), 185 (3), 147 (3), 91 (6), 84 (7), 57 (6). Calcd. for  $\text{C}_{29}\text{H}_{26}\text{N}_2$ : C 86.53, H 6.51, N 6.96; found: C 86.54, H 6.47, N 6.98%.

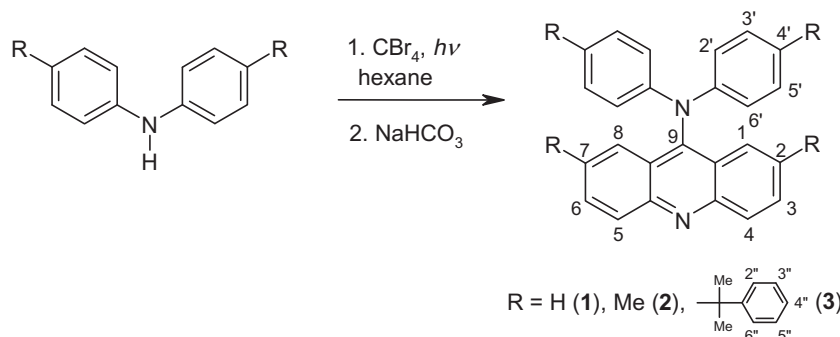
#### 2.2.3. 2,7-Bis(1-methyl-1-phenylethyl)-*N,N*-bis[4-(1-methyl-1-phenylethyl)phenyl]acridin-9-amine (**3**)

2,7-Bis(1-methyl-1-phenylethyl)-*N,N*-bis[4-(1-methyl-1-phenylethyl)phenyl]acridin-9-amine (**3**) was obtained as a yellow powder (yield 21%); m.p. 185–186 °C.  $^1\text{H}$  NMR ( $\text{CDCl}_3$ )  $\delta$ : 1.54 (s, 12 H, 4 Me), 1.67 (s, 12 H, 4 Me), 7.05 (d, 4 H, 2 H(2'), 2 H(6'),  $J = 8.5$  Hz), 7.11 (d, 4 H, 2 H(2''), 2 H(6''),  $J = 7.3$  Hz), 7.14 (d, 4 H, 2 H(3'), 2 H(5'),  $J = 8.5$  Hz), 7.16 (t, 2 H, 2 H(4''),  $J = 6.1$  Hz), 7.20 (m, 6 H, 2 H(3''), 2 H(4''), 2 H(5''), 7.25 (m, 8 H, 2 H(2''), 2 H(3''), 2 H(5''), 2 H(6''), 7.29 (br.d, 2 H, H(3), H(6),  $J = 9.2$  Hz), 8.02 (d, 2 H, H(4), H(5),  $J = 9.2$  Hz), 8.05 (br.s, 2 H, H(1), H(8)) ppm.  $^{13}\text{C}$  NMR ( $\text{CDCl}_3$ )  $\delta$ : 29.91 (4 Me), 30.71 (4 Me), 42.43 (2  $\text{CMe}_2$ ), 43.18 (2  $\text{CMe}_2$ ), 119.94 (2 C), 121.33 (4 C), 123.62 (2 C), 125.56 (2 C), 125.79 (2 C), 126.65 (4 C), 126.70 (4 C), 127.77 (4 C), 127.96 (4 C), 128.13 (4 C), 129.57 (2 C), 131.08 (2 C), 144.70 (2 C), 146.08 (2 C), 147.30 (2 C), 147.62 (C(9)), 149.38 (2 C), 149.47 (2 C), 150.54 (2 C) ppm. ESI MS  $m/z$ : 841.4492 (calc. for  $\text{C}_{61}\text{H}_{58}\text{N}_2 \cdot \text{Na}^+$ : 841.4498), 819.4672 (calc. for  $\text{C}_{61}\text{H}_{58}\text{N}_2 \cdot \text{H}^+$ : 819.4678). Calcd. for  $\text{C}_{61}\text{H}_{58}\text{N}_2$ : C 89.44, H 7.14, N 3.42; found: C 89.34, H 7.18, N 3.44%.

### 2.3. X-ray crystallography

Yellow crystals of compounds **1**, **2** were grown by slow evaporation of a solution in a mixture of  $\text{CH}_2\text{Cl}_2$ –hexane (~1:1, v/v) at room temperature. Purple crystals of salts **1**· $\text{HClO}_4$ , **3**· $\text{HClO}_4$  were grown by slow saturation of a MeCN–benzene solution (~1:1, v/v) of the compounds **1**, **3** in the presence of excess perchloric acid with a hexane–benzene mixture (~2:1, v/v) by the vapor diffusion method at room temperature. Single crystals of each of the compounds was coated with perfluorinated oil and mounted on a Bruker SMART CCD diffractometer (graphite monochromatized Mo  $K\alpha$  radiation,  $\lambda = 0.71073$  Å,  $\omega$ -scan mode) under a stream of cooled nitrogen.

All the structures were solved by direct methods and refined with full-matrix least-squares on  $F^2$  in anisotropic approximation for all non-hydrogen atoms (except for O atoms of disordered perchlorate anion in **1**· $\text{HClO}_4$  which were refined isotropically). The positions of hydrogen atoms at carbon atoms were calculated geometrically and then refined isotropically (for **2**), using a riding



Scheme 1.

model (for **1**·HClO<sub>4</sub>), or a mixed scheme (isotropically and a riding model for **1**, **3**·HClO<sub>4</sub>·MeCN). In protonated structures, the hydrogen atom at N(1) atom was located from the Fourier syntheses and then refined isotropically.

In structure **1**·HClO<sub>4</sub>, the Cl(1)O<sub>4</sub><sup>-</sup> ion is strongly disordered over four close positions with the ratio of occupancies 0.40:0.25:0.20:0.15 (rotation about Cl(1) atom). SADI command was applied to the oxygen atoms of this anion to constrain distances between them. In structure **3**·HClO<sub>4</sub>·MeCN, one of two PhCMe<sub>2</sub>C<sub>6</sub>H<sub>4</sub> fragments is disordered with the ratio of occupancies 0.55:0.45 and the phenyl substituent in the predominant conformer of this fragment is also disordered with the equal ratio of occupancies. SADI, ISOR, and AFIX66 commands were applied to constrain this disorder.

The calculations of the structures were performed using the SHELXTL-Plus software package [31]. Crystal data and data collections and refinement details are summarized in Table 1.

#### 2.4. Spectroscopic measurements

The absorption spectra were recorded on a Shimadzu UV-3101PC spectrophotometer. The absorption spectra of neutral forms of **1–3** were measured at room temperature in 1-cm quartz cells in solvents of different polarity. The concentrations used were in the range of  $7 \times 10^{-6}$  to  $9 \times 10^{-5}$  M. The absorption spectra of protonated forms of **1–3** were recorded in methanol with addition of 1 M HCl.

The fluorescence emission spectra were measured at 25 °C on a Fluorolog 3τ (Jobin Yvon, France) spectrofluorometer using a standard fluorescence 1-cm quartz cell in a temperature-controlled cell holder. The dye concentrations were selected at a sufficiently low level ( $10^{-5}$  M) in order to prevent the self-quenching effect. Before measurements, all solutions were deaerated by purging with argon for 3 min. The emission spectra were corrected for the wavelength-dependent response of the detection system measured with the help of the Calibration Kit Spectral Fluorescence Standards (Sigma-Aldrich, No. 97003). The excitation wavelength of 430 nm and spectral bandwidths of 3 and 1 nm for excitation and emission, respectively, were used.

The relative fluorescence quantum yields were determined according to the relationship:

$$\phi_s = \phi_r \frac{A_r F_s}{F_r A_s} \left( \frac{n_s}{n_r} \right)^2,$$

where  $\phi_r$  is the fluorescence quantum yield of a reference compound,  $A$  the absorbance,  $n$  the solvent refractive index, and  $F$  the area under the corrected fluorescence peak, the index ( $s$ ) means sample and ( $r$ ) means reference. Solution of fluorescein in 0.1 M NaOH ( $\phi_r = 0.9$ ) was used as a reference standard [32].

The fluorescence lifetimes were determined by a phase-modulation method using a Fluorog 3 Spectrofluorometer (Jobin Yvon, France).

#### 2.5. Measurements of chemosensor characteristics

Sensor films based on compound **2** were prepared by drop-casting toluene solutions containing polystyrene (5–10%) and **2** (2–5 mM) over a quartz plate. After solvent evaporation, the polymer-coated quartz plate was used as a cover of a cuvette containing a required solvent. The emission fluorescence spectra were taken from the back side of polymer films with an SD-2000 fiberoptic spectrofluorimeter equipped with a reflection/backscattering probe RP200-7 (Ocean Optics, USA). Upon exposure to saturated solvent vapor, the fluorescence signal was recorded as a function of time with an interval of 10–30 s.

#### 2.6. Computational details

Quantum-chemical calculations of free **1** and its protonated form **1**·H<sup>+</sup> were performed using density functional theory (DFT), which is a well-established method for calculating molecular structure. Electron transition energies ( $S_0$ – $S_1$ ) were calculated using time-dependent density functional theory (TD-DFT). In all calculations the PBE0 hybrid functional and Ahlrichs' double-zeta polarized SVP basis set were used [33]. Molecular geometries were optimized in DFT calculations for the ground electron state and in TD-DFT calculations for the excited electron state.

### 3. Results and discussion

#### 3.1. Synthesis and NMR studies

A proposed mechanism for the formation of acridine derivatives **1–3** is shown in Scheme S1 (see Supporting Information (SI) to this article). Compounds **1–3** were obtained in relatively low yields (16–21%). It seems that such low yields are conditioned by the formation of dark-colored, almost opaque reaction mixtures upon interaction of a diarylamine with CBr<sub>4</sub> that results in significant reaction rate retardation.

The 2D COSY and NOESY spectra of compounds **1–3** were used to assign the proton signals in <sup>1</sup>H NMR spectra (for example, see Figs. S1 and S2 in SI). Analysis of the NOESY spectra revealed that the cross peaks between acridine protons H(1), H(8) and phenyl protons H(2'), H(3'), H(5'), H(6') are very weak. This fact means that the distances between indicated protons are over 3 Å. Hence, the mean planes of diarylamino groups and the plane of acridine moiety are not parallel.

**Table 1**  
Summary of crystal data and structure refinement for **1**, **1**·HClO<sub>4</sub>, **2**, and **3**·HClO<sub>4</sub>·MeCN.

Structure	<b>1</b>	<b>1</b> ·HClO <sub>4</sub>	<b>2</b>	<b>3</b> ·HClO <sub>4</sub> ·MeCN
Empirical formula	C <sub>25</sub> H <sub>18</sub> N <sub>2</sub>	C <sub>25</sub> H <sub>19</sub> ClN <sub>2</sub> O <sub>4</sub>	C <sub>29</sub> H <sub>26</sub> N <sub>2</sub>	C <sub>63</sub> H <sub>62</sub> ClN <sub>5</sub> O <sub>4</sub>
Formula weight (g mol <sup>-1</sup> )	346.41	446.87	402.52	960.61
Color; shape	Yellow; plate	Purple; plate	Yellow; block	Purple; needle
Measured temperature (K)	173(2)	173(2)	120.0(2)	173(2)
Crystal system	Monoclinic	Orthorhombic	Triclinic	Triclinic
Space group	<i>P</i> 2 <sub>1</sub> / <i>c</i>	<i>Pbca</i>	<i>P</i> $\bar{1}$	<i>P</i> $\bar{1}$
Unit cell dimensions (Å, °)	<i>a</i> = 13.214(4) <i>b</i> = 8.764(3) <i>c</i> = 16.194(5) $\alpha$ = 90 $\beta$ = 107.779(5) $\gamma$ = 90	<i>a</i> = 9.248(9) <i>b</i> = 17.331(17) <i>c</i> = 26.24(3) $\alpha$ = 90 $\beta$ = 90 $\gamma$ = 90	<i>a</i> = 8.7616(5) <i>b</i> = 9.8458(5) <i>c</i> = 13.1903(7) $\alpha$ = 81.637(3) $\beta$ = 79.205(2) $\gamma$ = 89.956(3)	<i>a</i> = 8.546(3) <i>b</i> = 15.161(5) <i>c</i> = 20.127(7) $\alpha$ = 88.836(7) $\beta$ = 88.900(7) $\gamma$ = 84.880(7)
Volume (Å <sup>3</sup> )	1785.9(9)	4206(7)	1105.43(10)	2596.2(16)
<i>Z</i>	4	8	2	2
<i>D</i> <sub>x</sub> (g cm <sup>-3</sup> )	1.288	1.411	1.209	1.229
$\mu$ (mm <sup>-1</sup> )	0.076	0.218	0.07	0.126
Absorption correction	Not applied	Not applied	Not applied	Not applied
<i>F</i> (000)	728	1856	428	1020
$\theta$ Range (°)	2.64–28.99	2.48–29.00	1.59–29.00	2.39–30.63
Completeness to $\theta$ (%)	99.4	99.7	94.9	94.4
<i>h</i> , <i>k</i> , <i>l</i>	-18 ≤ <i>h</i> ≤ 18 -11 ≤ <i>k</i> ≤ 11 -22 ≤ <i>l</i> ≤ 21	-12 ≤ <i>h</i> ≤ 12 -23 ≤ <i>k</i> ≤ 23 -35 ≤ <i>l</i> ≤ 35	-11 ≤ <i>h</i> ≤ 11 -13 ≤ <i>k</i> ≤ 11 -17 ≤ <i>l</i> ≤ 17	-12 ≤ <i>h</i> ≤ 12 -21 ≤ <i>k</i> ≤ 21 -28 ≤ <i>l</i> ≤ 28
Reflections collected	16,881	39,380	8597	30,673
Reflections unique	4712 [R(int) = 0.0481]	5592 [R(int) = 0.1370]	5571 [R(int) = 0.0243]	15,127 [R(int) = 0.1196]
Unique reflections with <i>I</i> ≥ 2σ( <i>I</i> )	3034	2491	4415	5251
Number of parameters	308	322	384	956
Goodness-of-fit on <i>F</i> <sup>2</sup>	1.115	0.954	1.12	0.92
Final <i>R</i> indices [ <i>I</i> ≥ 2σ( <i>I</i> )]	<i>R</i> <sub>1</sub> = 0.0669, <i>wR</i> <sub>2</sub> = 0.1982	<i>R</i> <sub>1</sub> = 0.0858, <i>wR</i> <sub>2</sub> = 0.2375	<i>R</i> <sub>1</sub> = 0.0926, <i>wR</i> <sub>2</sub> = 0.2878	<i>R</i> <sub>1</sub> = 0.0827, <i>wR</i> <sub>2</sub> = 0.1218
<i>R</i> indices (all data)	<i>R</i> <sub>1</sub> = 0.1030, <i>wR</i> <sub>2</sub> = 0.2154	<i>R</i> <sub>1</sub> = 0.1863, <i>wR</i> <sub>2</sub> = 0.2742	<i>R</i> <sub>1</sub> = 0.1071, <i>wR</i> <sub>2</sub> = 0.2918	<i>R</i> <sub>1</sub> = 0.2406, <i>wR</i> <sub>2</sub> = 0.1686
Residual highest peak and deepest hole (e Å <sup>-3</sup> )	1.211, -0.172	1.351, -0.440	0.514, -0.477	0.240, -0.330

### 3.2. X-ray diffraction studies

The structures of compounds **1**, **2** and protonated forms **1**·HClO<sub>4</sub> and **3**·HClO<sub>4</sub> were determined by an X-ray diffraction analysis and are shown in Fig. 1. Selected geometric characteristics are presented in Table 2. It should be noted that information on crystallographic parameters of 9-diphenylaminoacridine and its derivatives is lacking in the Cambridge Crystallographic Database (version 5.32, 2011 release).

The results obtained show that the bond distances N(2)–C(7) (1.394–1.428 Å) are shorter than the typical single bond distance (1.46 Å), suggesting a conjugation of the diphenylamino group with the aromatic system of acridine. In all the structures, the sum of the bond angles around N(2) atom is close to 360°, thus indicating its *sp*<sup>2</sup> hybridization state. The dihedral angle N(1),C(1)...C(13)/N(2),C(7),C(14),C(20) ( $\alpha_1$ ) between the acridine and diphehylamine subunits varies in the range of 46–78°. This angle depends on the nature of the substituent groups and the charge state of a compound. For example, the acceptor and donor fragments in **1** are close to perpendicularity ( $\alpha_1 = 78^\circ$ ). Protonation leads to shortening of the N(2)–C(7) bond length (from 1.428 to 1.413 Å for compound **1**) and formation of a more planar conformation ( $\alpha_1$  decreases to 65° in **1**·H<sup>+</sup>).

The angles C(14)...C(19)/N(2),C(7),C(14),C(20) and C(20)...C(25)/N(2),C(7),C(14),C(20) ( $\alpha_2$  and  $\alpha_3$ ) indicating rotation of the phenyl groups vary over a range of 26–41°. It seems most probable that specific values of these angles are determined by the packing requirements of a compound.

### 3.3. Absorption spectra of neutral and protonated species

The UV–visible spectra of **1–3** were measured in different solvents at room temperature. For all the compounds, the absorption spectra in the region of 240–500 nm have similar structure and

consist of four bands. As an example, Fig. 2 shows the absorption spectrum of **1** in methanol with maxima at 249, 283, 362, and 453 nm.

It was found that the positions and molar extinctions of the first three short-wavelength bands of compounds **1–3** are nearly independent of the solvent polarity. By contrast, their unstructured long-wavelength absorption bands in the region of 450–460 nm exhibit small bathochromic shifts and decreases in the extinction with increase in solvent polarity. For example, for **1** the molar extinction coefficient is equal to 11,700, 10,700 and 10,300 M<sup>-1</sup>·cm<sup>-1</sup> in cyclohexane, 1,4-dioxane and DMSO, respectively. It is interesting that compound **3** having more bulky substituent groups exhibits higher extinction than **1** and **2** (17,400, 15,700 and 15,000 M<sup>-1</sup>·cm<sup>-1</sup> in cyclohexane, 1,4-dioxane and DMSO, respectively).

As seen, the second structured absorption band is centered at about 360 nm. It should be noted that this band is common to acridine and all its derivatives [6–8,12,15,23].

The existence of a broad structureless absorption band red-shifted relative to the 360-nm band is typical of all the aryl- and aminoaryl-substituted acridines, as well as corresponding acridinium systems [18]. According to Herbich et al. [11,14,15], 9-aminoarylacridines are donor–acceptor compounds containing aromatic amines as an electron donor and acridine as an acceptor. For these donor–acceptor compounds, the ICT leads to the appearance of low-energy charge-transfer absorption band. Note that 9-(4-aminophenyl)acridine containing aniline as an electron donor is the most widely studied compound of this type [11,12,14,15,22–24] and may therefore be considered as a reference donor–acceptor structure. Direct evidence that excitation of 9-(4-*N,N*-dimethylaminophenyl)acridine results in ICT followed by the appearance of acridine anion-radical transient spectra was obtained by picosecond flash photolysis [18]. Analogous results (the appearance of transient absorption spectra of aniline radical cation and acridinium

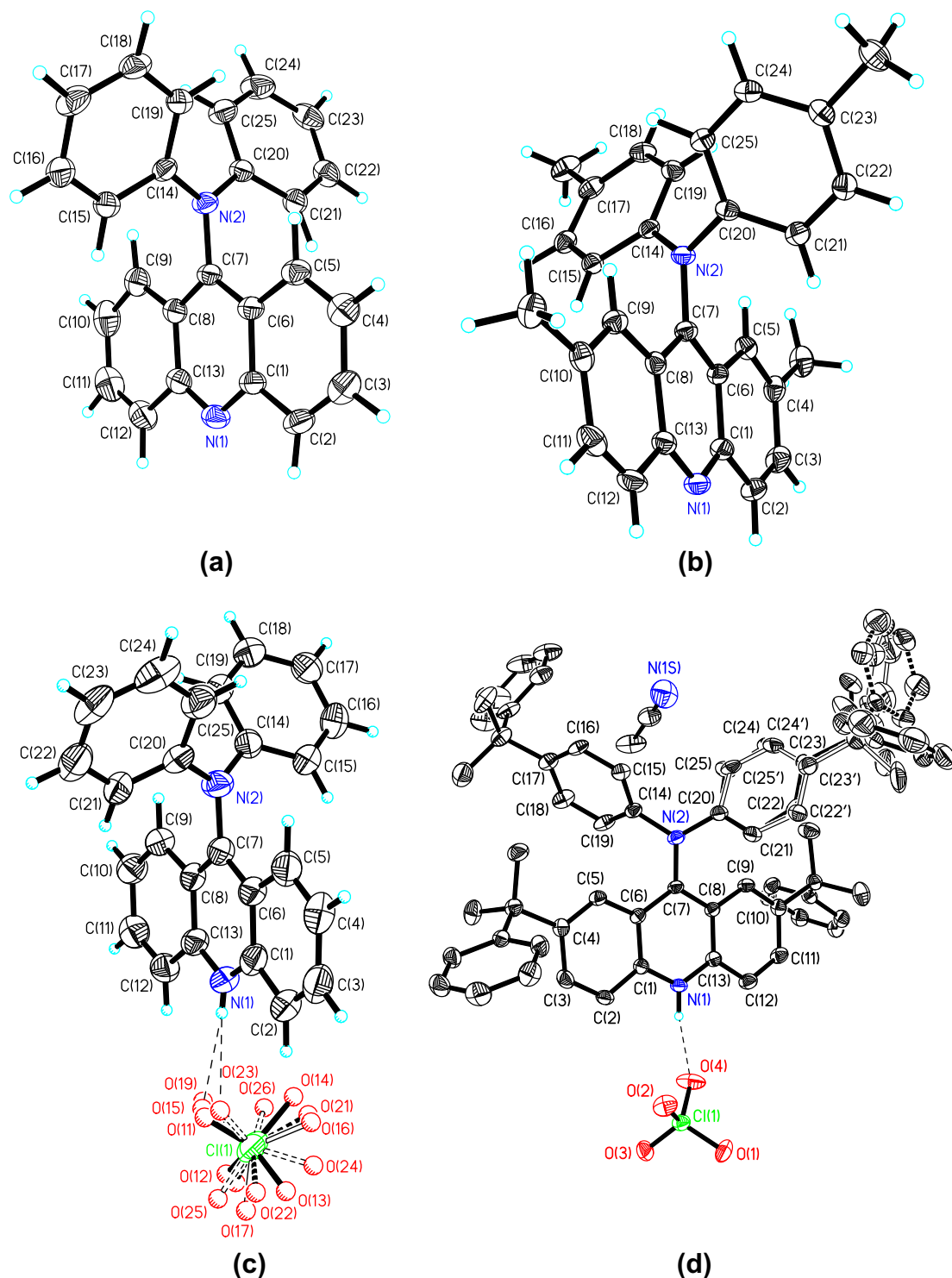


**Fig. 1.** Structures of (a) **1**, (b) **2**, (c) **1**·HClO<sub>4</sub>, and (d) **3**·HClO<sub>4</sub>·MeCN. All non-hydrogen atoms are shown at (a and d) 40% or (b and c) 50% probability of their thermal anisotropic displacement parameters (except for O atoms of the disordered anion in **1**·HClO<sub>4</sub>). In structure **3**·HClO<sub>4</sub>·MeCN, the most hydrogen atoms are not shown for clarity.

radical) were obtained earlier by Jones et al. for 10-methyl-9-(4-aminophenyl)acridinium ion by femtosecond laser flash photolysis [12].

Thus, the synthesized compounds **1–3** exhibit absorption spectra characteristic of typical donor–acceptor compounds.

Protonation of acridine nitrogen produces positively charged molecular ions **1**·H<sup>+</sup>–**3**·H<sup>+</sup>. It was stated that protonation of **1–3** changes insignificantly the position and shape of the UV bands in

the 250–400-nm region. At the same time the long-wavelength band in the region of 450–460 nm is considerably red-shifted further to the visible region. Fig. 3 shows the positions of two low-lying absorption bands of protonated forms of compounds **1–3** in acidic methanol.

As can be seen from the spectra, protonation results in considerable red shifts of the absorption bands (for example, about 70 nm for **1**). Experimental data show that the longest wavelength

**Table 2**  
Selected bond lengths (Å), bond and dihedral angles (°) in **1**, **1**·HClO<sub>4</sub>, **2**, and **3**·HClO<sub>4</sub>·MeCN.

Parameter	<b>1</b>	<b>2</b>	<b>1</b> ·HClO <sub>4</sub>	<b>3</b> ·HClO <sub>4</sub> ·MeCN
N(2)–C(7)	1.428(2)	1.424(4)	1.413(5)	1.394(3)
N(2)–C(14)	1.415(2)	1.423(5)	1.407(5)	1.433(4)
N(2)–C(20)	1.416(2)	1.430(4)	1.420(5)	1.426(4)
C(7)–N(2)–C(14)	117.5(2)	119.7(3)	120.0(3)	120.6(3)
C(7)–N(2)–C(20)	117.6(2)	117.6(3)	118.4(3)	120.2(3)
C(14)–N(2)–C(20)	124.9(2)	121.9(3)	121.5(3)	119.1(2)
Sum of bond angles about atom N(2)	360.0(2)	359.2(3)	359.9(3)	359.9(3)
N(1)H...OC(1)O <sub>3</sub>			2.03(5)–2.24(5) <sup>a</sup>	1.96(3)
N(1)–H...O			167(5)–174(5) <sup>a</sup>	168(3)
N(1),C(1)...C(13)/N(2),C(7),C(14),C(20)	78	65	68	46
C(14)...C(19)/N(2),C(7),C(14),C(20)	29	29	39	41
C(20)...C(25)/N(2),C(7),C(14),C(20)	26	40	40	38, 33 <sup>b</sup>
N(1),C(1)...C(13)/C(14)...C(19)	89	78	88	74
N(1),C(1)...C(13)/C(20)...C(25)	89	87	90	65, 68 <sup>b</sup>
C(14)...C(19)/C(20)...C(25)	50	63	67	70, 62 <sup>b</sup>

<sup>a</sup> For four conformers.

<sup>b</sup> For two conformers.

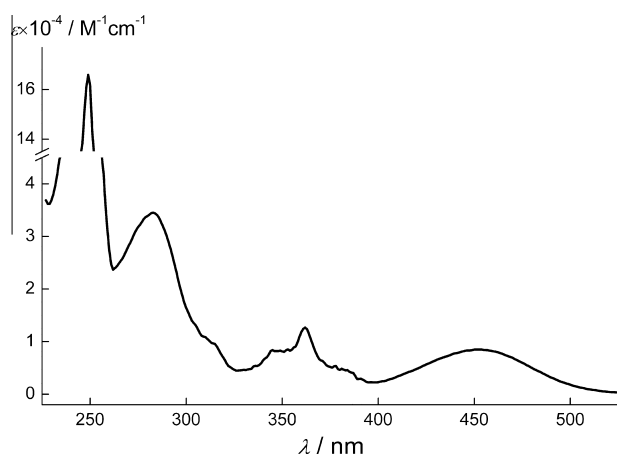


**Fig. 2.** Absorption spectrum of **1** in methanol.

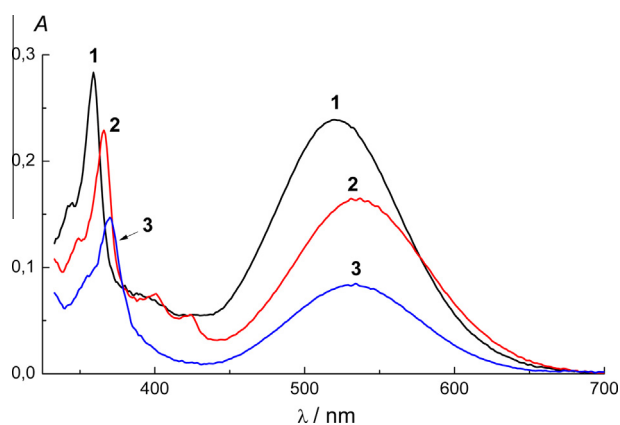


**Fig. 3.** Absorption spectra of protonated **1–3** ( $C = 1 \times 10^{-5}$  M) in methanol with added 1 M HCl.

absorption for **2**·H<sup>+</sup> and **3**·H<sup>+</sup> is somewhat longer than that for **1**·H<sup>+</sup>. It should be pointed out that compound **3** in the protonated form shows a lower extinction than protonated **1** and **2** ( $7000 \text{ M}^{-1} \text{ cm}^{-1}$  in comparison with  $20,200$  and  $15,200 \text{ M}^{-1} \text{ cm}^{-1}$  for **1**·H<sup>+</sup> and **2**·H<sup>+</sup>, respectively).

Note that similar red shifts upon protonation were observed by Mosurkal et al. [23] for 9-(4-aminophenyl)acridine which may be

considered as a reference donor–acceptor structure containing aniline as an electron donor. In addition, 10-methyl-9-(4-aminophenyl)acridinium ion was shown to have a wide absorption band with a maximum at about 530 nm [12].

### 3.4. Fluorescence properties

The fluorescence bands of neutral **1–3** in contrast to their absorption bands exhibit significant (up to  $3000\text{--}4500 \text{ cm}^{-1}$ ) red shifts on going from non-polar to polar solvents. Fluorescence spectra of three representative solutions, **1** in cyclohexane, 1,4-dioxane, and DMSO, are shown in Fig. 4. For compound **2**, more comprehensive red-shift data are given in Table 3.

To clarify how solvent–solute interactions affect the energy dissipation processes, the fluorescence quantum yields and decay times of **2** were measured as a function of the  $E_T(30)$  solvent polarity parameter [34]. Table 3 summarizes the solvent effects on the spectral position of the fluorescence maxima ( $\lambda_{\text{max}}^{\text{fl}}$ ), quantum yields ( $\varphi_{\text{fl}}$ ), decay times ( $\tau_{\text{fl}}$ ) and resulting radiative ( $k_r$ ) and non-radiative ( $k_{\text{nr}}$ ) rate constants of **2** at room temperature. The rate constants were calculated based on the equations  $k_r = \varphi_{\text{fl}}/\tau_{\text{fl}}$  and  $k_{\text{nr}} = (1 - \varphi_{\text{fl}})/\tau_{\text{fl}}$ .

The results listed in Table 3 show a decrease in the singlet excited state energy of **2** with increasing the  $E_T(30)$  value [34]. Similar results were obtained for compounds **1** and **3**. Compared to the cyclohexane solution, all other solutions of **1–3** show marked red shifts of the fluorescence bands. These results closely resemble those obtained by Herbich and Kapturkiewicz for 9-(dimethylaminophenyl)acridine and related compounds [15]. According to their interpretation, the marked solvent effect implies that the lowest singlet excited state of aminoarylacridines possesses charge-transfer character.

It is evident from the data in Table 3 that the fluorescence lifetime of **2** reduces parallel with the fluorescence quantum yield when solvent polarity increases. Nevertheless, the radiative rate constant decreases markedly with increasing solvent polarity. Note that similar effect was observed for 9-(dimethylaminophenyl)acridine [15]. The decrease in  $k_r$  proceeding toward polar solvents can be rationalized in terms of the Strickler and Berg equation [35] which predicts that the radiative rate constant decreases approximately as the cube of the emission wavenumber. Therefore, a smaller  $k_r$  is expected in polar solvent because of the red shift of the fluorescence spectrum. As in the case of hydroxy-substituted Nile Red, the increase in  $k_{\text{nr}}$  can be explained based on the energy gap law [36].

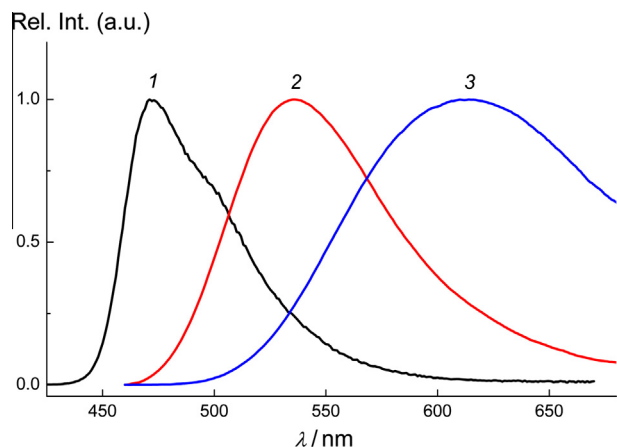


**Fig. 4.** Normalized room-temperature fluorescence spectra of **1** in (1) cyclohexane, (2) 1,4-dioxane, and (3) DMSO.

Protonated forms of **1–3** exhibit no fluorescence in acidic alcohol solutions that can be attributed to fluorescence quenching induced by hydrogen bonding. However, they do exhibit detectable fluorescence in the region of 630–650 nm in polymer films. As an example, Fig. 5 shows the fluorescence spectra of **3**·HBr formed in the course of photo-initiated synthesis from di[4-(1-methyl-1-phenylethyl)phenyl]amine and CBr<sub>4</sub> in polystyrene films (see Scheme S1 in SI).

Thus, the fluorescence spectra of protonated forms of **1–3** in polymer matrices are significantly (up to 100 nm) shifted to the longer wavelengths as compared to spectra of their neutral forms. It should be pointed out that this feature may be used for the development of fluorescent sensor materials changing their fluorescence from red to green upon exposure to ammonia vapors [30] as well as to vapors of other amines and pyridine.

### 3.5. Sensing properties

Solvatofluorochromic properties of **1–3** can be used to develop solvent-responsive sensor materials. Fig. 6 shows typical fluorescence responses of a thin polystyrene film doped with **2** upon exposure to saturated vapor of polar solvents. As can be seen, diffusion of analyte molecules (in this case molecules of toluene or chloroform) into dye-doped polymer matrices results in fluorescence quenching and progressive bathochromic shifts of the fluorescence maximum. The observed shifts and quenching are completely reversible. Measured emission shift and intensity change are characteristic of each analyte and can be used for its identification.

The use of protonated **2** as a fluorescent molecular sensor for recognition of proton-accepting compounds in the gas phase is

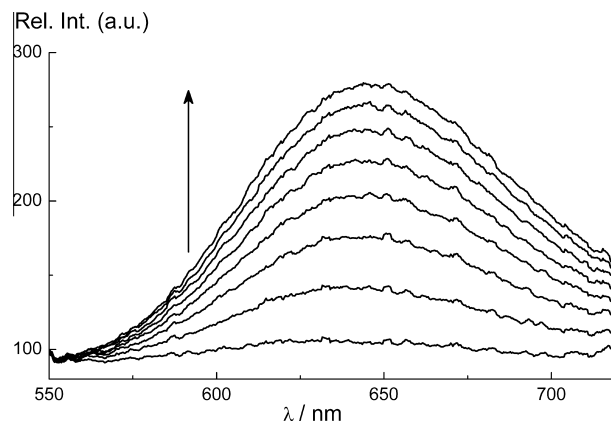


**Fig. 5.** Time-dependent fluorescence emission spectra of a polystyrene film containing di[4-(1-methyl-1-phenylethyl)phenyl]amine and CBr<sub>4</sub> upon exposure to UV light ( $\lambda = 375$  nm) at 0, 10, 20, 30, 40, 50, 60, and 70 s (bottom to top).

illustrated in Fig. 7. As seen, upon exposure to ammonia vapor the fluorescence maximum of a polystyrene film with immobilized **2**·H<sup>+</sup> shifts from 630 to 530 nm.

### 3.6. Results of DFT modeling

The structure and electronic properties of **1**, protonated form **1**·H<sup>+</sup> and electronically excited **1**<sup>\*</sup> were investigated theoretically by means of quantum mechanical calculations based on density functional theory (DFT) and time-dependent DFT (TD-DFT) using the PBE0 functional and SVP basis. Geometry optimizations were performed for the ground states of **1** and **1**·H<sup>+</sup>, and for the lowest excited state of **1**<sup>\*</sup>.

In Table 4, selected information regarding the calculated equilibrium state geometries for **1**, **1**·H<sup>+</sup> and **1**<sup>\*</sup> is presented.

As seen from Table 4, for **1** the predicted and measured bond lengths about atom N(2) agree reasonably well. Similarly, the DFT calculation predicts that for **1** the dihedral angles  $\alpha_1$ ,  $\alpha_2$ , and  $\alpha_3$  are 59°, 33° and 34°, respectively. These values compare favorably with the experimental values of 78°, 29° and 26°. Thus, the DFT-based equilibrium geometries in the ground state of **1** are close to these of experimental values.

For protonated form **1**·H<sup>+</sup>, DFT predicts that it must have shorter N(2)–C(7) bond length (1.371 Å instead of 1.415 Å), longer N(2)–C(14) and N(2)–C(20) bond lengths, smaller dihedral angle  $\alpha_1$  (42° instead of 59°) and larger angles  $\alpha_2$  and  $\alpha_3$ . This is in good agreement with obtained X-ray data. Note that for **3**·H<sup>+</sup> the measured values of N(2)–C(7) bond length and the dihedral angle are 1.394 Å and 46°, respectively. Thus, the DFT method correctly predicts the main geometrical changes involved in protonation of compounds **1–3**.

**Table 3**  
Photophysical properties of **2** in various solvents.

Solvent	$E_f(30)^a$ (kcal mol <sup>-1</sup> )	$\lambda_{\text{max}}^n$ ( $\nu_{\text{max}}^n$ ) nm (cm <sup>-1</sup> )	$\phi_f$	$\tau_f$ (ns)	$k_f \times 10^7$ (s <sup>-1</sup> )	$k_{nr} \times 10^7$ (s <sup>-1</sup> )
Cyclohexane	30.9	488 (20,500)	0.57	29.3	1.95	1.47
Toluene	33.9	529 (18,900)	0.30	27.0	1.11	2.59
1,4-Dioxane	36.0	558 (17,900)	0.27	24.2	1.12	3.02
THF	36.2	575 (17,400)	0.15	18.9	0.79	4.50
Chloroform	39.1	592 (16,900)	0.13	18.0	0.72	4.83
Acetone	42.2	618 (16,200)	0.06	12.5	0.48	7.52
DMSO	45.1	641 (15,600)	0.02	10.2	0.20	9.61
Acetonitrile	45.6	633 (15,800)	0.03	7.8	0.38	12.4
2-Propanol	48.4	623 (16,000)	0.008	7.2	0.11	13.78

<sup>a</sup> See Ref. [34].

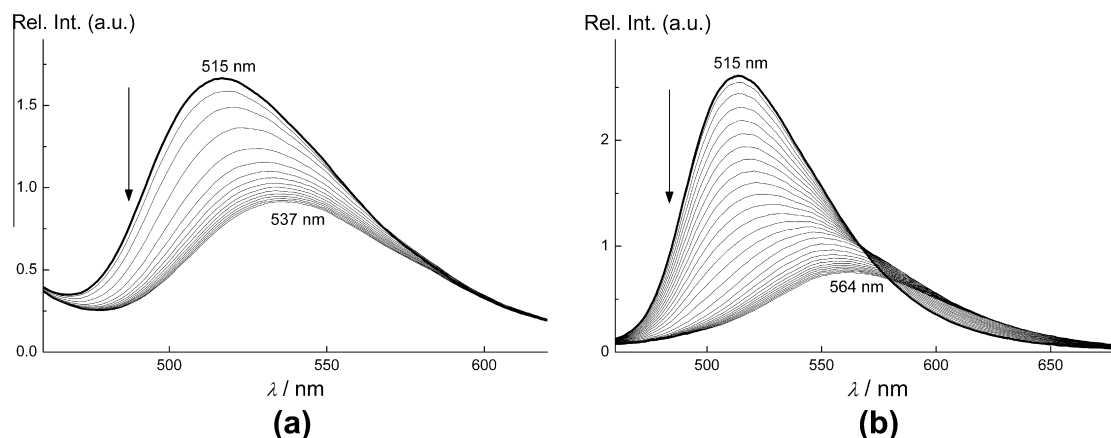


**Fig. 6.** Time-dependent fluorescence spectra of polystyrene films (thickness  $\sim 20 \mu\text{m}$ ) doped with **2** upon exposure to saturated vapors of (a) toluene and (b) chloroform ( $\lambda_{\text{exc}} = 375 \text{ nm}$ , room temperature). Spectra were recorded at every 10 s from the beginning of exposure (top to bottom).

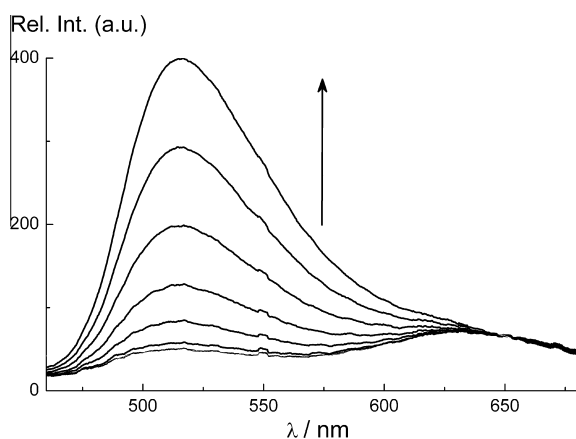


**Fig. 7.** Time-dependent fluorescence spectra of a polystyrene film containing **2** upon exposure to ammonia saturated vapor ( $\lambda_{\text{exc}} = 375 \text{ nm}$ , room temperature). Spectra were recorded at every 10 s from the beginning of exposure (bottom to top).

It should be pointed out that similar results were obtained by Mosurkal et al. [23] and by Lappe and co-workers [22] for 9-(4-aminophenyl)acridine. At the DFT/B3LYP/6-31G<sup>\*</sup> level of theory, geometry changes associated in protonating 9-(4-aminophenyl)acridine include shortening of the bond length from 1.49 to 1.46 Å for the bond connecting the acridine moiety and the phenyl group and a decrease in the dihedral angle between the acridine moiety and the attached phenyl group from 66° to 52° [23].

It is worth noting that DFT predicts a trend to oppose changes in geometry upon excitation of **1** as compared to those upon protonation: the calculated dihedral angle  $\alpha_1$  is increased from 59° to 87°, the N(2)–C(7) bond distance is elongated up to 1.447 Å, whereas the N(2)–C(14) and N(2)–C(20) bond lengths and angles  $\alpha_2$  and  $\alpha_3$  are reduced. This statement is clearly illustrated in Fig. S3 (SI). Note that this is in general agreement with the TICT hypothesis based on the assumption of a perpendicular conformation of two

structural subunits in the first excited state of donor–acceptor compounds (for example, anthryl and acrydyl derivatives of dimethylaniline [15,18,37]). It should be mentioned, however, that excited-state conformational transformations of such compounds are still a matter of controversy. For example, Herbich and Kap-turkiewicz based on their experimental data have concluded that conformation of 9-aminoarylacridines in fluorescent state is more planar than that in the ground state [15].

The results of TD-DFT-based modeling of absorption and emission behavior of **1** are presented in Table 5 and Fig. 8.

As seen from Table 5, calculated absorption bands for **1** involve excitations between the three high-lying occupied orbitals (HOMO, HOMO-1, HOMO-2) and the two low-lying unoccupied orbitals (LUMO, LUMO+1). The topology of the four frontier molecular orbitals is shown in Fig. S4 (SI). Structural transformations on going from **1** to **1**·H<sup>+</sup> and **1**<sup>\*</sup> discussed above result in shifts of the HOMO and LUMO energy levels and, as a consequence, in decreases of corresponding transition energies. As seen, protonation lowers the gap between the HOMO and the LUMO for **1**·H<sup>+</sup> compared to **1** (from 3.46 to 3.12 eV) and this is reflected in the increase in calculated absorption wavelength from 449 to 472 nm. Similarly, excitation reduces significantly (up to 2.98 eV) the HOMO–LUMO energy gap for **1**<sup>\*</sup> in comparison with **1** due to a decrease of the LUMO energy level and an increase of the HOMO level. As a result, the calculated gas-phase S<sub>0</sub>–S<sub>1</sub> transition for **1**<sup>\*</sup> is shifted to 584 nm. Note, that in both cases the predicted trends are in line with experimental results, although there are some discrepancies between calculated and measured values.

It should be pointed that TD-DFT calculations for the emission band of the protonated form **1**·H<sup>+</sup> gave unreasonable strongly underestimated transition energy, which is evidently due to known deficiencies of the TD-DFT method in the case of charge-transfer transitions.

For **1**, the calculations suggest that the main contribution to the lowest energy absorption in the region of 450 nm is the HOMO–LUMO transition, whereas the second band at 360 nm is mainly due to the electronic transition from HOMO-1 to LUMO. The results

**Table 4**  
Bond lengths (Å) and dihedral angles (°) for neutral **1**, protonated form **1**·H<sup>+</sup> and electronically excited **1**<sup>\*</sup> calculated at PBE0/SVP level of theory. Experimental values are given in parentheses.

Compound	N(2)–C(7)	N(2)–C(14)	N(2)–C(20)	Dihedral angle $\alpha_1$	Dihedral angles $\alpha_2, \alpha_3$
<b>1</b>	1.415 (1.428)	1.411 (1.415)	1.413 (1.416)	59 (78)	33, 34 (29, 26)
<b>1</b> ·H <sup>+</sup>	1.371 (1.413)	1.426 (1.407)	1.433 (1.420)	42 (68)	42, 49 (39, 40)
<b>1</b> <sup>*</sup>	1.447	1.377	1.397	87	21, 33

**Table 5**

Electronic excitation energies and corresponding oscillator strengths ( $f$ ), main configurations and weight coefficients of the electronically excited states of **1** and **1-H<sup>+</sup>** calculated by TD-DFT/PBE0/SVP based on the optimized ground and excited state geometries. The experimental values of absorption and fluorescence maxima of **1** in cyclohexane solution and absorption of **1-H<sup>+</sup>** in methanol are also included.

Compound	Transition	Orbitals involved (individual excitation weight)	HOMO energy level (eV)	LUMO energy level (eV)	$\lambda_{\text{calc}}$ (nm/eV)	$f$	$\lambda_{\text{exp}}$ (nm)
<b>1</b>	$S_0 \rightarrow S_1$	HOMO $\rightarrow$ LUMO (0.944)	-2.21	-5.67	449/2.76	0.119	455
	$S_0 \rightarrow S_2$	HOMO-1 $\rightarrow$ LUMO (0.921)			347/3.57	0.079	369
	$S_0 \rightarrow S_3$	HOMO $\rightarrow$ LUMO + 1 (0.603)			293/4.23	0.087	286
		HOMO-2 $\rightarrow$ LUMO (0.370)					
<b>1-H<sup>+</sup></b>	$S_0 \rightarrow S_1$	HOMO $\rightarrow$ LUMO (0.970)	-6.09	-9.21	472/2.63	0.307	521
	$S_0 \rightarrow S_2$	HOMO-1 $\rightarrow$ LUMO (0.935)			382/3.24	0.044	359
<b>1<sup>+</sup></b>	$S_0 \rightarrow S_1$	HOMO $\rightarrow$ LUMO (0.990)	-2.56	-5.54	584/2.12	0.019	488

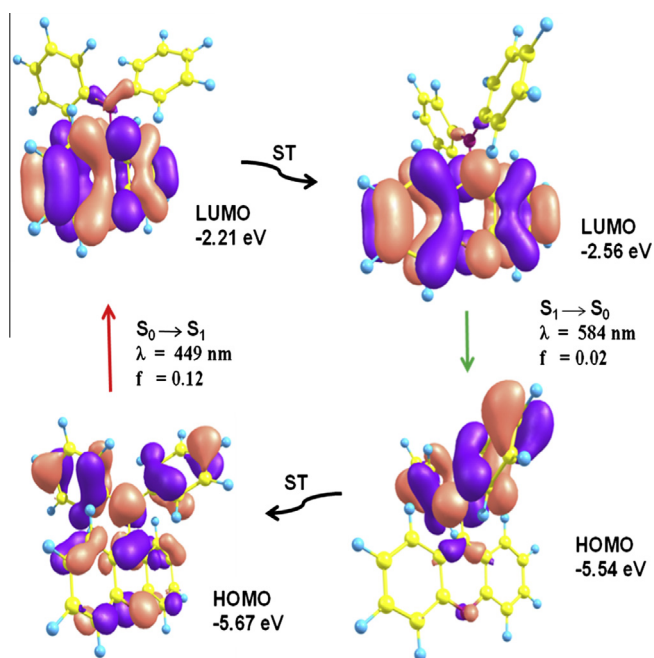


**Fig. 8.** Topology and energies of frontier orbitals for **1** and **1<sup>+</sup>** calculated at the PBE0/SVP level of theory. Red and green arrows represent excitation and emission, respectively. ST refers to structural transformation. (For interpretation of the references to colour in this figure legend, the reader is referred to the web version of this article.)

obtained show that HOMO is localized mainly on the diphenylamino moiety, whereas the HOMO-1 and the LUMO are localized on the acridine core. Fig. 8 shows the topology of the frontier molecular orbitals involved in the vertical excitation and emission of **1**. It is interesting that the electron-transfer nature of the  $S_0 \rightarrow S_1$  transition is clearly recognized in the case of **1<sup>+</sup>** for which the LUMO and HOMO are almost fully localized on the acceptor and donor moieties, respectively.

Thus, DFT-based calculations predict that the  $S_0 \rightarrow S_1$  transition in **1** is basically a charge-transfer excitation connected with charge transfer from diphenylamino fragment to acridine moiety. On the other hand, the fact that the HOMO-1 and LUMO are localized predominantly in acridine unit explains why the position and shape of the second band at 360 nm are similar in all aryl- and aminoaryl derivatives of acridine and acridinium ion.

#### 4. Conclusions

We have synthesized three new acridine dyes of donor–acceptor type, studied the structure and spectral characteristic of their

neutral and protonated forms and performed DFT-based modeling calculations.

It was found that the synthesized dyes are nonplanar in their ground state, whereas a pronounced trend toward planarity takes place upon protonation. The synthesized compounds show low-energy charge-transfer fluorescence bands which undergo red-shifts with increasing solvent polarity. The observed increase of the shift with increasing solvent polarity indicates the charge-transfer character of the relaxed fluorescent state in polar environment. The protonation of the dyes extended their UV–visible absorption and fluorescence spectra further into visible region.

It was shown that observed structural features and electronic properties of the dyes can be accurately described within the TD-DFT framework. For the ground state, DFT predicts a strong tendency to coplanarity upon protonation, that is in good agreement with the obtained experimental data. Calculations show that in all cases electronic excitation from  $S_0$  to  $S_1$  corresponds to the HOMO–LUMO transition. Protonation reduces the HOMO–LUMO energy gap, thus accounting for the observed increase in absorption wavelength upon protonation. Geometry optimization performed for the first excited state indicates a tendency for obtaining a more orthogonal conformation upon excitation.

Both neutral and protonated 9-diarylaminoacridines may be used as fluorescent molecular sensors and may be applied to examine the structure, dynamics and microenvironment in heterogeneous and biological systems.

#### Appendix A. Supplementary material

CCDC 848689 (**1**), 848690 (**1-HClO<sub>4</sub>**), 848691 (**2**), and 848692 (**3-HClO<sub>4</sub>-MeCN**) contain the supplementary crystallographic data for this paper. These data can be obtained free of charge via <http://www.ccdc.cam.ac.uk/conts/retrieving.html> (or from the Cambridge Crystallographic Data Center, 12, Union Road, Cambridge CB2 1EZ, UK; fax: +44 1223 336033). Supplementary data associated with this article can be found, in the online version, at <http://dx.doi.org/10.1016/j.molstruc.2013.09.001>.

#### References

- [1] W.A. Denny, *Curr. Med. Chem.* 9 (2002) 1655.
- [2] V.A. Bacherikov, T.-C. Chou, H.-J. Dong, X. Zhang, C.-H. Chen, Y.-W. Lin, T.-J. Tsai, R.-Z. Lee, L.F. Liu, T.-L. Su, *Bioorg. Med. Chem.* 13 (2005) 3993.
- [3] R. Kumar, M. Singh, D.N. Prasad, O. Silicari, S. Sharma, *Chem. Sci. Trans.* 2 (2013) 246.
- [4] J. Joseph, E. Kuruvilla, A.T. Achuthan, D. Ramaiah, G.B. Schuster, *Bioconjugate Chem.* 15 (2004) 1230.
- [5] H. Gao, W.A. Denny, R. Garg, C. Hansch, *Chem. Biol. Interact.* 116 (1998) 157.
- [6] K. Kasama, K. Kikuchi, S. Yamamoto, K. Uji-ie, Y. Nishida, H. Kokubun, *J. Phys. Chem.* 85 (1981) 1291.
- [7] K. Kasama, K. Kikuchi, Y. Nishida, H. Kokubun, *J. Phys. Chem.* 85 (1981) 4148.
- [8] K. Kikuchi, K. Kasama, A. Kanemoto, K. Uji-ie, H. Kokubun, *J. Phys. Chem.* 89 (1985) 868.
- [9] J. Herbich, A. Kapturkiewicz, *Chem. Phys.* 158 (1991) 143.

- [10] J. Rak, J. Blazejowski, J. Photochem. Photobiol. A 67 (1992) 287.
- [11] J. Herbich, A. Kapturkiewicz, Chem. Phys. 170 (1993) 221.
- [12] G. Jones II, M.S. Farahat, S.R. Greenfield, D.J. Gosztola, M.R. Wasielewski, Chem. Phys. Lett. 229 (1994) 40.
- [13] J.J. Aaron, M. Maafi, C. Parkanyi, C. Boniface, Spectrochim. Acta 51A (1995) 603.
- [14] J. Herbich, A. Kapturkiewicz, Chem. Phys. Lett. 273 (1997) 8.
- [15] J. Herbich, A. Kapturkiewicz, J. Am. Chem. Soc. 120 (1998) 1014.
- [16] O. Rubio-Pons, L. Serrano-Andrés, M. Merchán, J. Phys. Chem. A 105 (2001) 9664.
- [17] D. Citterio, K. Minamihashi, Y. Kuniyoshi, H. Hisamoto, S. Sasaki, K. Suzuki, Anal. Chem. 73 (2001) 5339.
- [18] Z.R. Grabowski, K. Rotkiewicz, W. Rettig, Chem. Rev. 103 (2003) 3899.
- [19] S. Fukuzumi, H. Kotani, K. Ohkubo, S. Ogo, N.V. Tkachenko, H. Lemmetyinen, J. Am. Chem. Soc. 126 (2004) 1600.
- [20] I. Negron-Encarnación, R. Arce, M. Jiménez, J. Phys. Chem. A 109 (2005) 787.
- [21] J.W. Verhoeven, H.J. van Ramesdonk, H. Zhang, M.M. Groeneveld, A.C. Benniston, A. Harriman, Int. J. Photoenergy 7 (2005) 103.
- [22] J. Lappe, R.J. Cave, M.D. Newton, I.V. Rostov, J. Phys. Chem. B 109 (2005) 6610.
- [23] R. Mosurkal, L. Hoke, S.A. Fossey, L.A. Samuelson, J. Kumar, D. Waller, R.A. Gaudiana, J. Macromol. Sci. A 43 (2006) 1097.
- [24] G. Jones II, D. Yan, J. Hu, J. Wan, B. Xia, V.I. Vullev, J. Phys. Chem. B 111 (2007) 6921.
- [25] S. Fukuzumi, Phys. Chem. Chem. Phys. 10 (2008) 2283.
- [26] M. Hoshino, H. Uekusa, A. Tomita, S. Koshihara, T. Sato, S. Nozawa, S. Adachi, K. Ohkubo, H. Kotani, S. Fukuzumi, J. Am. Chem. Soc. 134 (2012) 4569.
- [27] V.A. Sazhnikov, A.G. Strukov, M.G. Stunzhas, S.P. Efimov, O.M. Andreev, M.V. Alfimov, Dokl. Akad. Nauk USSR 288 (1986) 172 (in Russian).
- [28] V.A. Sazhnikov, A.A. Khlebunov, M.V. Alfimov, High Energy Chem. 41 (2007) 25.
- [29] V.A. Sazhnikov, M.V. Alfimov, Chem. Eng. Trans. 15 (2008) 267.
- [30] M.V. Alfimov, V.A. Sazhnikov, A.A. Khlebunov, D.S. Ionov, A.N. Petrov, V.M. Aristarkhov, A.Y. Men'shikova, N.N. Shevchenko, A.V. Yakimansky, Optical chemical sensors on the base of arrays of ink-jet printed micro- and nanoparticles, in: Technical Proceedings of the 2009 NSTI Nanotechnology Conference, May 3–7, 2009, vol. 1, Houston, Texas, USA, pp. 554–557.
- [31] SHELXTL-Plus, version 5.10, Bruker AXS Inc., Madison, WI, USA, 1997.
- [32] M.D. Galanin, A.A. Kutyonkov, V.N. Smorchkov, Y.P. Timofeev, Z.A. Chizhikova, Optika i Spektroskopiya (Opt. Spectrosc.) 53 (1982) 683 (in Russian).
- [33] A. Schaefer, H. Horn, R. Ahlrichs, J. Chem. Phys. 97 (1992) 257.
- [34] C. Reichardt, Solvents and Solvent Effects in Organic Chemistry, third ed., Wiley-VCH, Weinheim, 2003.
- [35] S.J. Strickler, R.A. Berg, J. Chem. Phys. 37 (1962) 814.
- [36] K. Nagy, S. Göktürk, L. Biczók, J. Phys. Chem. A 107 (2003) 8784.
- [37] A. Siemiarczuk, Z.R. Grabowski, A. Krówszyński, M. Asher, M. Ottolenghi, Chem. Phys. Lett. 51 (1977) 315.